Physical Chemistry - Lund University

Master Thesis

Orientation of Sticks and Spheres - Estimating Tensor Shape and Orientation Distribution using Diffusion NMR

Author:
Mikael Leveau Novén

Supervisor:
Professor Daniel Topgaard

A thesis submitted in fulfilment of the requirements for the degree of Master of Science in Engineering

in the

Diffusion NMR methods development group
Physical Chemistry

July 2015

"So, ultimately, in order to understand nature it may be necessary to have a deeper understanding of mathematical relationships. But the real reason is that the subject is enjoyable, and although we humans cut nature up in different ways, and we have different courses in different departments, such compartmentalization is really artificial, and we should take our intellectual pleasures where we find them."

Richard Feynman

LUND UNIVERSITY

Abstract

Engineering Faculty
Physical Chemistry

Master of Science in Engineering

Orientation of Sticks and Spheres - Estimating Tensor Shape and Orientation Distribution using Diffusion NMR

by Mikael Leveau Novén

The diffusion characteristics of water can be measured by using NMR methods. Specifically, the diffusion profiles in samples containing domains of water barriers are of major importance to be able to describe in applications such as diffusion tensor imaging or diffusion MRI-sequences. These sequences can be used to study the internal structure of samples of complex diffusion profiles. The diffusion characteristics can be described by a diffusion tensor matrix which can be parameterised by the isotropic diffusion coefficient and the level of anisotropy. This thesis work aims to measure diffusion weighted NMR signals from a triple-stimulated spin-echo pulse sequence to simultaneously determine both the diffusion tensor characteristics and the orientation density function, ODF. Traditionally, obtaining the ODF is based on assuming a fixed diffusion tensor in a diffusion-weighted NMR experiment to describe the different signal attenuations along different directions as differences in the shape of the microscopic water domains. By the work presented in this report, it is proven by measurements on lyotropic liquid crystal systems that the shape of the diffusion tensor and the ODF indeed can be extracted from the same measurement. This is shown for samples having either prolate or oblate diffusion tensors.

Acknowledgements

I would like to express my sincere appreciation to all the people who have helped me during my years of learning. To all teachers, professors, and fellow students whom have helped me grow and learn. To all the love and support I have gotten from family and friends. Without you this thesis could never have been written.

A very warm thank you to Stefanie Eriksson who has supported me for the entirety of this master thesis work, teaching both handling the NMR spectrometer and the theory behind the diffusion-weighted NMR experiments along with giving well-needed feedback on results and this report. Göran Carlström has, with an angel's patience, helped in setting the NMR spectrometer in order and getting it to work when it didn't want to. Last, but certainly not least, I am extremely grateful to professor Daniel Topgaard for the chance of doing this work and for the support and guidance along the way.

Contents

List of Figures

List of Tables

Abbreviations

AD	**A**xial **D**iffusion
dMRI	**d**iffusion **M**agnetic **R**esonance **I**maging
DT	**D**iffusion **T**ensor
DTI	**D**iffusion **T**ensor **I**maging
DW-MRI	**D**iffusion-**W**eighted **M**agnetic **R**esonance **I**maging
FA	**F**ractional **A**nisotropy
FID	**F**ree **I**nduction **D**ecay
NMR	**N**uclear **M**agnetic **R**esonance
ODF	**O**rientation **D**istribution **F**unction
PAS	**P**rincipal **A**xis **S**ystem
RD	**R**adial **D**iffusion
TriPGSTEbp	**Tri**pple-**ST**imulated **P**ulsed-**G**radient **E**cho sequence with **bip**olar gradient pulse pairs

Summary

Mapping the inside: Study of water diffusion using NMR experiment

This work shows how the internal structures of samples, which for instance could be cells or crystals, containing microscopic water channels and other structures where the water molecules can move in some directions but not in others can be determined in detail by looking at the magnetic properties of atomic nuclei. In order to see the structures in which the water molecules can move, two kinds of information about how the molecules move around are needed. First, the way in which the water molecules can move inside of the channels, i.e. the diffusion of water, must be known. Second, the difference in how the water molecules can move around depending on the direction within the sample must be known. Older ways of finding out the latter depends on guessing the former. The technique described in this work shows a way to determine both in the same measurement.

When you measure temperature with a thermometer it is the motion of molecules that is measured. Every molecule in a liquid moves around freely and randomly while still bumping into other molecules. This motion of molecules is called diffusion. Nuclear magnetic resonance (NMR) spectroscopy is the study of how the magnetic properties of atomic nuclei change from the influences of magnetic fields. As all nuclei are found within molecules and the molecules move around, it is understandable that the NMR signal can change if the molecules move around. In my work, I have shown that a NMR method can be used to map the diffusion of water molecules inside samples that have thin channels or corridors that the water molecules can move around in. Similar methods are used to map diffusion of water in the neurons in the brain, which among other things can show how the neurons are connected. The new thing that I showcase in my report, is that it is possible to determine two important features of the sample; both how much the water diffusion only can occur in one direction and also which directions the channels and corridors are oriented in. Previously, it has not been possible to determine both based on the same measurement. This improvement is important as it helps to make the map of the channel orientations more reliable. In the future, this might be used to study samples which is has a complex microscopical environment where the water molecules move around in wide or narrow corridors, big halls, and across planes. One very important application of this could be to gain more understanding of both the

types, conditions, and structure of cells and tissues of the brain if the experiment could be performed in a clinical MRI scanner.

ffl (1)

1. Introduction

The study of samples in which diffusion of water is limited in some directions and less in others, i.e. showing anisotropic diffusion profiles, using diffusion weighted nuclear magnetic resonance, diffusion NMR, is an area of intense research [1–3]. Diffusion NMR experiments are useful in that they can be used to study diffusion characteristics of sensitive samples non-invasively, which is the key factor of its importance as a tool for diagnosis of pathological conditions as well as the anatomy of healthy tissues [4, 5]. If combined in imaging sequences, diffusion NMR techniques are generally collected under the name of diffusion tensor imaging, DTI, and diffusion-weighted magnetic resonance imaging, DW-MRI [6]. The techniques are especially useful to study white matter in the brain, mainly consisting of bundled axons called nerve fibers, where DTI and DW-MRI can be used to assess anatomical information such as axon diameter, dendrite density, and degree of myelination [7] [8, 9]. By studying the difference in diffusion along different directions, the orientations of the nerve fibers in a voxel, three dimensional pixel, can be determined and described by an orientation distribution function, ODF [10, 11]. The ODF was introduced in the field of magnetic resonance neuroimaging to deal with the fact that previous methods could not account for crossing fibers within a voxel [12]. Diffusion in microscopic domains can be described by a diffusion tensor. It has recently been shown that by varying the way in which diffusion is encoded into the NMR signal, the level of microscopic anisotropy, i.e. the shape of the microscopic diffusion tensor, can be calculated [3]. This technique has been shown to provide a possible way of distinguishing between different kinds of brain tumors [4]. One problem of studying diffusion using NMR techniques is that it requires long sequences of magnetisation manipulation using magnetic gradients. Even as the studied signal is dependent on excitation states that last for time-scales from milliseconds up to seconds the interactions between the studied nuclei and other nuclei in the sample cause signal loss, an effect known as transversal or T_2-relaxation [13]. This can cause a problem in diffusion-weighted NMR

experiments in which the magnetisation must be manipulated for long periods of time to encode effects of diffusion into the signal.

The aim of this thesis is to investigate the possibility of determining both the diffusion tensor characteristics and orientation distribution function based on data gathered from a recently developed diffusion NMR experiment encoding both directional and isotropic diffusion called the triple-stimulated stimulated-echo diffusion NMR experiment ,TriPG-STEbp [14, 15]. Determining the shape of the diffusion tensor prior to calculating the ODF is important as techniques currently in use to determine the ODF rely on a priori guesses of the shape of the diffusion tensor. This will inflict errors in the estimations of the channel orientations based on the ODF [16, 17]. The determination of the shape of the diffusion tensor is possible due to the recent discovery that the encoding of diffusion is not only possible along on single direction but also equally in all spatial directions, isotropically, in an elegant and fast way [14].This novel technique could prove useful in future medical applications as it could provide important anatomical and physiological information from brain tissue in a non-invasive way. Also, study of more complex systems consisting of microscopic water domains can be characterised. As model sample, water, surfactant and oil was mixed in ratios providing supramolecular structures of micro- to millimeter scale water channels of various orientations. Such samples have been well-studied in the context of diffusion NMR [1, 15, 18–20]. Despite relatively short T_2-values, diffusion weighting is possible in three dimensions using the stimulated echo-strategy [15]. To validate the orientation density function obtained, a standard DTI experiment was performed on each studied sample and an ODF was constructed from the DTI data. Also, the imaging sequence was used to ensure that the sample was homogenous as the diffusion characteristics is provided for each voxel within the sample, which the non-imaging sequence TriPGSTEbp does not show.

2. Diffusion Tensor

Samples containing microscopic domains of water, e.g. biological tissue or lyotropic crystals, can be examined using diffusion NMR techniques which encode the self-diffusion of water in the domains within the sample. For samples showing diffusion anisotropy, which are of particular interest to study, it is necessary to describe diffusion in three dimensions. The apparent diffusion of water in three dimensions are described by the diffusion tensor. Diffusion anisotropy is the characteristics of diffusion not being equal in three dimensions. The diffusion tensor, in turn, can be parameterised in a number of ways of which the most important are described below. Tensors are used to describe a quantity of a physical property. In the simplest case, a case in which the property has no direction or gradient, a physical property can be described as a scalar. This corresponds to a tensor of rank 0. On the other hand, a property that has a magnitude in one direction, such as a velocity, is described by a tensor of rank 1, meaning that the tensor has one non-zero eigenvalue. The diffusion tensor of a sample with microdomains of water is described by a second order tensor of rank 3, having 3 non-zero eigenvalues, shown in 2.1 [21]

$$\mathbf{D} = \begin{pmatrix} D_{xx} & D_{xy} & D_{xz} \\ D_{yx} & D_{yy} & D_{yz} \\ D_{zx} & D_{zy} & D_{zz} \end{pmatrix}. \tag{2.1}$$

If the laboratory frame of reference and the tensor principle axis system, PAS, coincide, D is symmetric and the off-diagonal elements are zero. The mean diffusivity, MD or $\bar{D}$, can be written as the mean of the diagonal elements of the diffusion tensor matrix,

$$\bar{D} = \frac{Tr(\mathbf{D})}{3} = \frac{D_{xx} + D_{yy} + D_{zz}}{3} = \frac{\lambda_1 + \lambda_2 + \lambda_3}{3}, \tag{2.2}$$

where $\lambda_1, \lambda_2 \text{and} \lambda_3$ are the eigenvalues of the diffusion tensor, also known as the principal diffusivities [22]. There are many ways of parameterising the diffusion tensor. Below

follows the definition necessary to understand the experiments and analyses used in this thesis report. The apparent diffusion coefficient, D_θ or ADC, of a cylindrically symmetrical sample observed in a standard PGSE experiment is defined by the angle, θ, between the PGSE gradient and the main axis of symmetry of the lamellar or reverse hexagonal phase as

$$D_\theta = D_\parallel \cos^2\theta + D_\perp \sin^2\theta, \tag{2.3}$$

where $D_\parallel$ and $D_\perp$ are the self diffusion coefficients parallel and perpendicular to the direction of the gradient . $D_\parallel$ and $D_\perp$ are also called the Axial, AD, and Radial, RD, diffusion coefficients, respectively [23]. For samples containing domains of different orientations the distribution of orientations, $P(D)$, can, if random distribution of domains is assumed, be written as [20]

$$P(D) = \frac{1}{2\sqrt{(D - D_\perp)(D_\parallel - D_\perp)}}. \tag{2.4}$$

where D are the apparent diffusion coefficient for a given direction. Also, and of major importance in this thesis project, the diffusion tensor can, in its PAS, be parametrized into

$$D_{\text{iso}} = \frac{D_{xx} + D_{yy} + D_{zz}}{3}, \tag{2.5}$$

$$D_\Delta = \frac{1}{3D_{\text{iso}}}\left(D_{zz} - \frac{D_{yy} + D_{xx}}{2}\right), \tag{2.6}$$

$$D_\eta = \frac{D_{yy} - D_{xx}}{2D_{\text{iso}}D_\Delta}, \tag{2.7}$$

where D_{iso} is the isotropic value, D_Δ the anisotropy and asymmetry, D_η [15]. The elements are ordered into $|D_{zz} - D_{\text{iso}}| > |D_{xx} - D_{\text{iso}}| > |D_{yy} - D_{\text{iso}}|$ out of convention. Due to the choices of numerical factors, the parameters are within the range of $-0.5 \leq D_\Delta \leq 1$ and $0 \leq D_\eta \leq 1$. Axial symmetry, $D_\eta = 0$, will be assumed for the rest of this report. The value of D_Δ gives the shape of the diffusion tensor where negative, 0, and positive means oblate, spherical, and prolate tensors, respectively. Figure 2.1 shows the conceptual shapes of diffusion tensors of anisotropy values from -0.5 to 1. To get complete grasp of the diffusion tensor parameterisations used in this report, the connection between AD and RD and D_{iso} and D_Δ is

$$D_\perp = D_{\text{iso}}(1 - D_\Delta) \tag{2.8}$$

and

$$D_{\parallel} = D_{\text{iso}}(1 + 2D_{\Delta}). \tag{2.9}$$

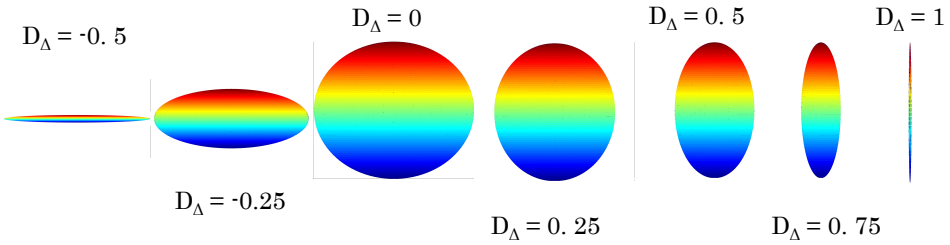

FIGURE 2.1: Conceptual shapes of diffusion tensors with anisotropies, D_{Δ}, ranging from -0.5 (furthest left) and +1 (furthest right). The extreme D_{Δ} values, -0.5 and 1, are given some three dimensional extension to make them visible although they should have no thickness. Colours of the tensor shows position along the z-axis, blue as lowest and red as highest.

An alternative description of the relative amount of anisotropic diffusion in a sample is the fractional anisotropy, FA, index which compares the magnitude of the diffusion tensor to the magnitude of the anisotropic part of the diffusion tensor [24]. The magnitude of the diffusion tensor is given by the generalised tensor product

$$\sqrt{\mathbf{D} : \mathbf{D}} = \sqrt{\sum_{i=1}^{3}\sum_{j=1}^{3} D_{ij}^2}, \tag{2.10}$$

while the anisotropic part of $\mathbf{D}$ is given by

$$\sqrt{D : D} = \sqrt{\sum_{i=1}^{3}\sum_{j=1}^{3} (D_{ij} - \bar{D}I_{ij})^2}, \tag{2.11}$$

where I_{ij} denotes the ij-element of the identity tensor. FA can thus be written

$$\text{FA} = \sqrt{\frac{3}{2}}\frac{\sqrt{D : D}}{\sqrt{\mathbf{D} : \mathbf{D}}}. \tag{2.12}$$

Yet another model of diffusion anisotropy, commonly used in DTI, depends on the rank of the diffusion tensor in each voxel, linear anisotropy, CL, spherical anisotropy, CS, and planar anisotropy, CP, [2]. Each voxel can be described by a composition of the three anisotropy measures. If the eigenvalues are ordered as $\lambda_1 > \lambda_2 > \lambda_3$ CL and CP are

defined as

$$\mathrm{CL} = \frac{\lambda_1 - \lambda_2}{\lambda_1} \tag{2.13}$$

and

$$\mathrm{CP} = \frac{(\lambda_2 - \lambda_3)}{\lambda_1}. \tag{2.14}$$

A high value of CL indicate that diffusion along a channel is dominant while a high value of CP indicates that diffusion along a geometric plane dominates. High value of CL would indicate prolate diffusion tensor ($D_\Delta > 0$) while a high value of CP would indicate more of an oblate diffusion tensor ($D_\Delta < 0$).

3. Diffusion NMR

NMR spectroscopy is based on the effect of a strong magnetic field on the individual spins of atomic nuclei. Specifically, nuclei that have non-zero spin that is recognised by a measurable magnetic moment and angular momentum. For a thorough introduction on NMR spectroscopy, the reader is referenced to textbooks such as [13] as this section will be limited to remind the reader of a few important concepts. The first of these concepts is that the angular frequency with which the magnetic angular moment of a nucleus rotates under influence of a homogenous external magnetic field, B_0 (T), depends on the gyromagnetic ratio of the studied nucleus, γ (rad T^{-1} s^{-1}). This frequency is called the Larmor frequency, ω_0 (rad s^{-1}), and is given by

$$\omega_0 = \gamma B_0. \tag{3.1}$$

As a convention, the orientation of B_0 is defined as the z-axis. For spatial encoding of the spinning magnetisation vectors, a magnetic field gradient, $\mathbf{G}$ (T m^{-1}), is applied over the sample. This means that depending on the position of the spins within the sample, the effective frequency of the precession of the spin will be different. Accordingly, the spins will be out of phase with spins in other locations within the sample in a predictable fashion. In the simplest case, the gradient is applied perpendicular to B_0 and the cumulative phase shift, $\phi(t)$ (rad), can be described as

$$\phi(t) = \gamma B_0 t + \gamma \int_0^t G(t')z(t')dt', \tag{3.2}$$

where t is the time during which the gradient along the z-axis, $G(t)$, is applied and $z(t)$ is the time-dependent position of the nucleus along the z-axis [25]. The application of well-defined magnetic gradients is the basis for both imaging and diffusion NMR techniques. For diffusion NMR, the positions of the spins are first encoded by applying

a gradient pulse. For a predetermined time, the diffusion time, the nuclei will move due to random thermal motion, diffusion, unaffected by gradients. This will put them out of the positions in which their frequency has been encoded. Thereafter, the position encoding gradient is reapplied but in the opposite direction to rephase the spins. However, because the nuclei have moved out of position, the rephasing will be imperfect and thus the recorded signal will be lower than if the nuclei had not moved. This reduction can be studied to determine the diffusion characteristics of the molecules containing the studied nuclei, as will be shown and described in more detail in this chapter. The recordable NMR signal is called the Free Induction Decay, FID. The signal decays due to that the magnetic moment vector reorients to the B_0 direction, a phenomenon called longitudinal relaxation, and the effects of fluctuations in the local magnetic field around the nucleus which dephase the spinning nuclei, which is called the transversal relaxation. T_2 denotes a decay constant for the magnetisation perpendicular to the B_0 direction.

3.1 Pulsed Gradient Spin Echo Pulse Sequence

A simple example of a diffusion NMR experiment is the pulse-gradient spin-echo sequence, PGSE [26] [27]. An overview of this sequence is found in figure 3.1. The function of the 180-degree inversion pulse is to remove the dephasing of the spins due to magnetic inhomogeneities in the sample or the applied magnetic fields. The expression for the signal intensity for a pulse-gradient spin-echo sequence is given by

$$I(b) = I(0)e^{-bD}, \tag{3.3}$$

where

$$b = (\gamma G\delta)^2(\Delta - \delta/3), \tag{3.4}$$

where b is the diffusion-weighting variable, $I(0)$ is the signal with no applied magnetic gradient, and D is the diffusion coefficient of the studied nucleus. The diffusion coefficient can be calculated by comparing the signal from multiple PGSE sequences with varying G magnitude, δ, or Δ. However, in samples with short T_2 times, i.e. the spins dephase quickly in the x-y-plane, it is useful to instead of applying one 180^o apply two 90^o pulses in succession, allowing diffusion between them. It is necessary for the spins to be in the xy-plane during times in which they are diffusion-encoded by the applied gradients.

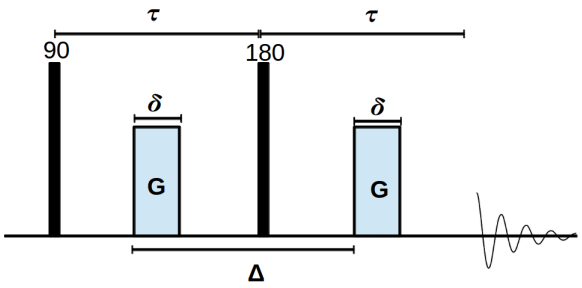

FIGURE 3.1: A pulsed-gradient spin-echo pulse sequence with two equal magnetic gradients, G, of duration δ between the 90-degree pulse and the 180-degree echo pulse. Δ denotes the time from the leading edges of the gradient pulses and is also the time during which diffusion can affect signal attenuation and is hence called the diffusion time. Signal acquisition is performed at the echo time, 2τ, is indicated by the decaying sinusoidal curve to the right in the figure.

This strategy is referred to as "z-storage" as the signal is stored along the z-axis during the diffusion time. Spin-echo sequences dividing the 180-pulse into two 90-pulses are called stimulated-echo sequences, an example of which is shown in figure 3.2. Although equation 3.3 gives the signal for encoding of diffusion in one dimension, the underlying theory is viable for diffusion encoding in all spatial dimensions.

3.2 Three Dimensional Diffusion NMR

In order to obtain information about translational motion in all three spatial dimensions, the NMR signal can be encoded using a three dimensional magnetic gradient, $\mathbf{G}^T(t)$, that varies with time [14]. This gives rise to a dephasing vector, $\mathbf{q}(t)$

$$\boldsymbol{G}^T(t) = \{G_x(t), G_y(t), G_z(t)\}, \tag{3.5}$$

$$\mathbf{q}(t) = \gamma \int_0^t \mathbf{G}(t')dt'. \tag{3.6}$$

The diffusion weighting matrix, $\mathbf{b}$ is given by

$$\mathbf{b} = \int_0^\tau \mathbf{q}(t)\mathbf{q}^T(t)dt, \tag{3.7}$$

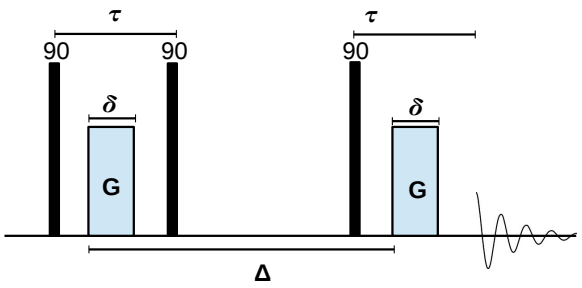

FIGURE 3.2: A pulsed-gradient stimulated-echo pulse sequence with two equal magnetic gradients, G, of duration δ between the first and second 90-degree pulse and after the third 90-degree pulse. The first 90-degree stores the magnetisation along the z-axis, making it invulnerable to transversal relaxation during most of Δ. Signal acquisition is indicated by the decaying sinusoidal curve to the right in the figure. This is the important difference compared to the pulsed-gradient spin echo experiment described in figure 3.1.

where τ is the echo time at which the spin magnetisation is rephased. As recently shown, the b-matrix can be characterised by the total diffusion weighting b, anisotropy b_Δ, and asymmetry b_η [15]

$$\begin{aligned} b &= b_{xx}^{PAS} + b_{yy}^{PAS} + b_{zz}^{PAS}, \\ b_\Delta &= \frac{1}{b}(b_{zz}^{PAS} - \frac{b_{yy}^{PAS} + b_{xx}^{PAS}}{2}),, \\ b_\eta &= \frac{3}{2}\frac{b_{yy}^{PAS} - b_{xx}^{PAS}}{b b_\Delta}, \end{aligned} \tag{3.8}$$

where PAS denotes the principal axis system of the tensor. Interestingly, by varying the angles at which the q-vector is spun the b-parameters shown in equation 3.8 can be controlled independently of each other. This is achieved through control of applied magnetic gradients that build the q-vector, see 3.6.

If Gaussian diffusion can be assumed, the recorded signal amplitude can be described as

$$I = I_0 \cdot e^{-\mathbf{b}:\mathbf{D}}, \tag{3.9}$$

where I_0 corresponds to the signal intensity at no applied gradient and $\mathbf{b} : \mathbf{D}$ denotes the generalised scalar product as defined as

$$\boldsymbol{b} : \mathbf{D} = \sum_i \sum_j b_{ij} Dij, \tag{3.10}$$

which, in the b-matrix's PAS, can be written as

$$\boldsymbol{b} : \mathbf{D} = b_{xx}^{PAS} D_{xx} + b_{yy}^{PAS} D_{yy} + b_{zz}^{PAS} D_{zz}. \tag{3.11}$$

In the parameterisation shown in equation 3.8 is used and axially symmetric diffusion-encoding is used, i.e. $b_\eta = 0$ and the diffusion tensor has axial symmetry, $D_\eta = 0$, equation 3.11 can be written as

$$\boldsymbol{b} : \mathbf{D} = bD_{\text{iso}}[1 + 2b_\Delta D_\Delta P_2(\cos\beta)], \tag{3.12}$$

where β is the angle between the z-axis unit vectors of the b and D vectors PAS, $\mathbf{n_b}$ and $\mathbf{n_D}$, respectively,

$$\cos\beta = \mathbf{n_b} \cdot \mathbf{n_D}. \tag{3.13}$$

3.3 Diffusion Tensor Imaging Experiment

Obtaining spin echo sequence data in slices along some axis in the sample allows for mapping the diffusion characteristics of the sample [28]. By phase encoding in two directions, x and y, and frequency encoding in the z-direction, spatial resolution is obtained. By repeating the experiment with incrementations of the phase encoding gradient strengths, a 3D image with contrast given by the FA value, described in equation 2.12, and color coded to show the directionality of the diffusion tensor parameters can be constructed. Diffusion encoding is performed by using a diffusion encoding gradient, G_{diff}. The increments of the gradient strengths of G_{diff} give rise to changes in signal attenuation in accordance with equation 3.9. If the total time the spins are subjected to transverse relaxation is longer than the average T_2 for a voxel, the DTI data from that voxel will be non-representative. To compensate for the effects of the T_2 relaxation, a map of the T_2 values for each voxel can be measured. By only using the voxels in which T_2 are long enough to ensure a signal to be obtained, the data is ensured to

provide reliable results of diffusion encoding. T_2 can be measured in a sample voxel per voxel and shown as a T_2 image which can, if using the same imaging settings as for the standard DTI experiment, be used to mask the DTI data unusable for ODF production. For details on how this is performed, see chapters 4 and 6.

The ODF and DTI obtained using this method can be used to compare to the ODF resulting from the triple-stimulated spin-echo pulse sequence as it offers a visualisation of the diffusion tensor both in the resulting diffusion tensor image and through the constructed ODF.

3.4 Triple-stimulated echo pulse sequence with bipolar gradient pulse pairs

The strength of the triple-stimulated echo sequence with bipolar gradient pulse pairs, TriPGSEbp, is that it allows for equal diffusion encoding in three successive direction [14]. The sequence is shown in figure 3.3. For each gradient direction, a stimulated echo is carried out, assuring that the total time for T_2-relaxation is limited to as short time as possible, in total $6\tau_1$. Even in stimulated echo experiments, transverse relaxation occurs during times in which the spins are in the xy-plane, i.e. during diffusion encoding. The reason for choosing bipolar gradients is to mitigate effects of internal gradients and eddy currents. Eddy currents are induced currents in surrounding conducting material of the NMR-spectrometer which, in turn, induce magnetic fields that distort the gradient fields [29]. The directions in which the stimulated blocks encode the signal for diffusion are given by,

$$\mathbf{n}_i = \begin{bmatrix} x_i \\ y_i \\ z_i \end{bmatrix} = \begin{bmatrix} \cos\psi_i \sin\zeta \\ \sin\psi_i \sin\zeta \\ \cos\zeta \end{bmatrix}, \tag{3.14}$$

where ζ is the inclination angle and ψ_i is the azimuthal angle of the unit vectors of the gradient directions. The vectors are symmetrically spaced around the z-axis. This means that

$$\psi_i = \frac{2\pi}{3}(i-1), i = 1, 2, 3, \tag{3.15}$$

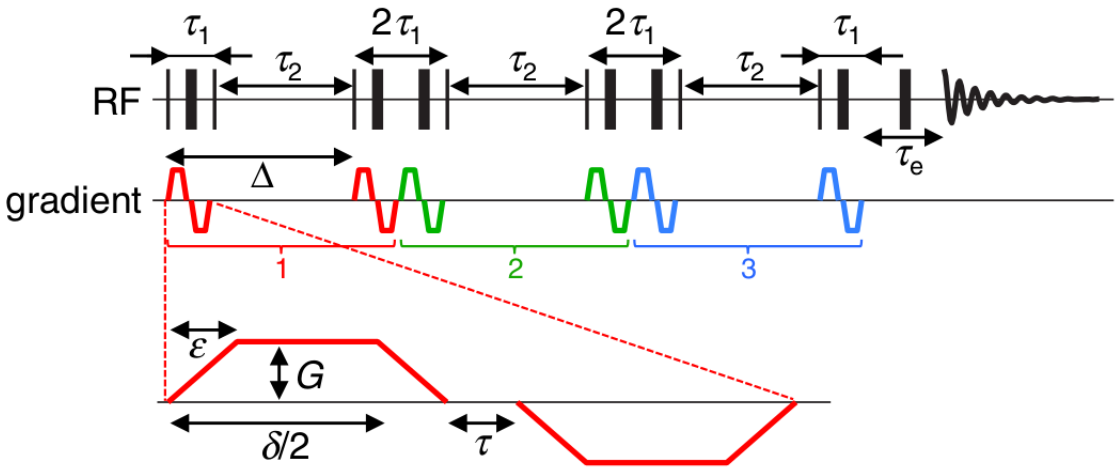

FIGURE 3.3: The triple-stimulated echo pulse sequence with bipolar gradient pulse pairs. In the radio frequency, RF, pulse line, thin and broad lines correspond to 90^o_x and 180^o_y pulses, respectively. The colours of the gradient pulses correspond to the direction of the gradient. Taken with consent from [14]

ζ can be used to encode diffusion with various directional information.

$$\begin{aligned} b_{xx} = b_{yy} &= b\frac{\sin^2\zeta}{2} \\ b_{zz} &= b\cos^2\zeta, \\ b_{xy} = b_{yx} = b_{xz} = b_{zx} = b_{yz} = b_{zy} &= 0 \end{aligned} \tag{3.16}$$

where b is the diffusion weighting matrix defined by the pulse sequence parameters found in figure 3.3

$$b = 3(\gamma G\delta)^2\big(\Delta - \frac{\delta}{3} - \frac{\tau}{2} - \frac{\epsilon}{2} - \frac{\epsilon^2}{6\delta} + \frac{\epsilon^3}{15\delta^2}\big). \tag{3.17}$$

At the so-called "magic angle", $\text{acos}(\frac{1}{\sqrt{3}})$ isotropic diffusion encoding is achieved as the b-tensor can be written as

$$b_{xx} = b_{yy} = b_{zz} = b/3. \tag{3.18}$$

Also, it is useful to notice that truly directional diffusion encoding is achieved at $\zeta = 0$ where

$$b_{xx} = b_{yy} = 0, \tag{3.19}$$

$$b_{zz} = b. \tag{3.20}$$

The resulting signal is, if powder-averaged, dependent on the diffusion tensor as well as on the b-matrix as

$$I(b, b_\Delta) = I_0 e^{-bD_{\text{iso}}} \frac{\sqrt{\pi}}{2} \frac{e^{bD_{\text{iso}} b_\Delta D_\Delta}}{\sqrt{3bD_{\text{iso}} b_\Delta D_\Delta}} \text{erf}\Big(\sqrt{3bD_{\text{iso}} b_\Delta D_\Delta}\Big), \tag{3.21}$$

or, described as $D_\parallel$ and $D_\perp$, [14]

$$\frac{I}{I_0} = \frac{\sqrt{\pi}}{2} \frac{e^{-bD_\perp}}{\sqrt{b(D_\parallel - D_\perp)}} \text{erf}\Big(\sqrt{b(D_\parallel - D_\perp)}\Big). \tag{3.22}$$

By fitting simulated signals based on estimations of D_{iso} and D_Δ and the knowledge of the used b-matrix to the recorded data, the values of D_{iso} and D_Δ can be obtained. Repeating the sequence in a number of directions of the symmetry axis of the b-matrix gives a chance of obtaining a representative powder-averaged signal as well as an ODF. The data acquired in the TriPGSTEbp experiment provides diffusion weighted signals from multiple directions of the gradient frame which are evenly distributed in three dimensions based on the electrostatic repulsion scheme [30]. Figure 3.4 shows a conceptual figure of the process of determining the ODF of a sample through analysis of the TriPGSTEbp data as shown above. Both the isotropically and directionally diffusion weighted signal is powder-averaged in order to obtain the same signal to noise ratio. The isotropically diffusion weighted signal, however, should be the same independent on the measured direction.

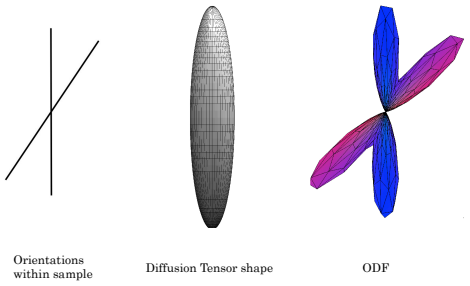

FIGURE 3.4: Example of DT and ODF estimation of a sample with anisotropic diffusion domains, channels, along two different directions (left). As diffusion NMR measurements are made along various directions, the shape of the DT (centre) is estimated, and by using the signal of various directions and the DT shape, the fiber ODF can be calculated.

4. Orientation Distribution Function

As useful as the diffusion tensor model is, it lacks in that it does not describe the spread of orientations of structures in which self-diffusion is dominant. This is especially troublesome in DTI experiments carried out on samples where multiple fiber orientations can exist within the resolution attainable by current diffusion weighted MRI-techniques, such as brain tissue. One application in which it is of uttermost importance to correctly determine the direction of the underlying fibers is fiber tracking in which nerve fiber tracks are traced by examining the diffusion profile of the whole or part of the brain, voxel per voxel [31]. The first strategy of obtaining the fiber tracks was by assuming that the direction of the dominant eigenvector shows the average fiber direction within the voxel. However, at the current obtainable spatial resolutions, each voxel might contain fiber populations that cross, making approaches based on tracking the dominant eigenvector insufficient [11]. The term "fiber" originates from the DTI application of neural fiber tracking and is, in this report, interchangeable with any kind of channels within which the apparent diffusion coefficient of water is much greater in one direction than in others. The challenges of disparate orientations within one voxel can be tackled by some different strategies such as q-ball imaging and high angular resolution diffusion imaging (HARDI) experiments [32, 33]. Experiments that are designed to produce ODFs can either stop at determining the diffusion ODF, which represents the motion of water molecules, or the fiber ODF, which attempts to represent the fiber orientations [34]. However, the calculation of the fiber ODF is currently dependent on guessing the shape of the diffusion tensor to adjust the diffusion ODF to only account for the directions along which the diffusion tensor is prolate. The data acquired in the TriPGSTEbp experiment provides diffusion weighted signals from multiple directions of the gradient frame which are evenly distributed in three dimensions based on the electrostatic repulsion scheme [30]. This means that both diffusion tensor characterisation, as shown in the diffusion NMR-chapter, and ODF reconstruction is possible from data from the same experiment.

An approach to describe an unknown number of orientations of fibers within a voxel is the Orientation Distribution Function, ODF, also called Orientation Density Function or Fiber Orientation function [10]. Orientations are given in spherical coordinates where θ is the inclination angle and ϕ is the azimuthal angle. θ is defined to be along the z-axis. It is here useful to see the factors after the b value in equation3.12 as an effective diffusion value, D_{eff}. The ODF, $P(\theta, \phi)$, gives the fraction of the fibers oriented along a certain direction, (θ, ϕ) and is related to the diffusion-weighted signal attenuation as

$$\frac{I(\mathbf{b})}{I_0} = \int_0^{\pi} \int_0^{2\pi} K(\mathbf{b}, D_{\text{iso}}, D_{\Delta}, \theta, \phi) P(\theta, \phi) d\theta d\phi, \tag{4.1}$$

where

$$K(\mathbf{b}, D_{\text{iso}}, D_{\Delta}, \theta, \phi) = e^{-bD_{\text{eff}}}, \tag{4.2}$$

and

$$D_{\text{eff}} = D_{\text{eff}}\big(1 + 2b_{\Delta} D_{\Delta} \mathrm{P}_2(\cos\beta)\big), \tag{4.3}$$

where β is the angle between the z-axis unit vectors of the b and D vectors PAS as given by equation 3.13 and P_2 is the 2^{nd} Legendre polynomial

$$\mathrm{P}_2(x) = \frac{3x^2 - 1}{2}. \tag{4.4}$$

It is noteworthy that β will be dependent on θ and ϕ

Solving equation 4.1 to obtain $P(\theta, \phi)$ can be achieved by using a kernel based on the most anisotropic voxels in the data[10]. The major strength of the TriPGSTEbp experiment is that it measures both D_{iso} and D_{Δ} directly, thus making it possible to directly and correctly build the correct fiber ODF based on the diffusion tensor shape via D_{eff}. This means that all the information needed to describe the kernel is obtained in one experiment. To obtain the ODF the signal attenuation is discretised onto a spherical mesh and solve the problem using a non-negative least-squares fit of equation 4.1 [35]. The plotted ODF is the mean of multiple obtained ODFs from random sampling of the TriPGSTEbp data using bootstrap resampling.

5. Lyotropic Liquid Crystals

Lyotropic liquid crystalline materials consist of molecules that self-assemble into supermolecular structures who possess a long-range orientational order when a solvent is introduced. Typically, and in the context of this report, the constituents of the lyotropic crystals are amphiphilic molecules, water, and oil. Depending on the concentration ratios of the constituents, the structure of the crystalline phases differ [36]. For studying anisotropic diffusion, lamellar and reverse hexagonal phases are of most interest as the water molecules can, ideally, only diffuse in one direction or a plane, respectively. Conceptual figures of the lamellar and reverse hexagonal phases are found in figure 5.1.

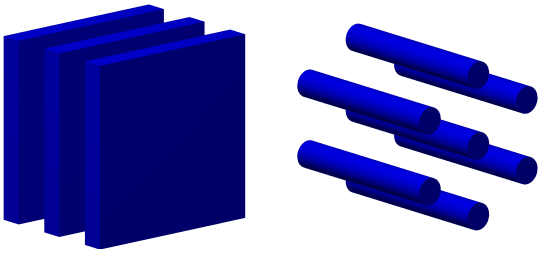

FIGURE 5.1: Conceptual figure showing the sheet structure in lamellar phase (left) and the water channels in reverse hexagonal phase (right) lyotropic liquid crystals.

Lyotropic liquid crystals are used in diffusion NMR because of the control that is attainable over the shape of micro- and millimeter-scale structures of water barriers [1, 15, 18–20]. Magnetic fields are known to be able to orient liquid lyotropic crystals if these show an anisotropy in magnetic susceptibility of aggregated structures [37, 38]. The effective anisotropic magnetic susceptibility is a summation of contributions from the molecular components including the aliphatic chains, such as in the dioctyl sodium sulfosuccinate molecule or $C_{14}E_5$ used as surfactant in the studied samples in this work. This means that the magnetic field induces a torque on the molecules within its effect. In liquid lyotropic crystal systems, the alignment effect can be immediately observed if the sample is heated to an isotropic phase and allowed to cool to a reversed hexagonal phase

while within the magnetic field. Alignment can be observed in field strengths of a few T for molecules of high anisotropy in magnetic susceptibility. The control of anisotropic diffusion domains, i.e. the structures of water barriers, the availability of the substrates, and the fact of it being a well-studied system makes the AOT/H_2O/iso-octane liquid crystal system a good choice for using in a diffusion NMR experiment.

6. Materials & Methods

This chapter describes the equipment, methods and samples used for the experimental work and data analysis.

6.1 Simulations

Data from the TriPGSTEbp experiment can be used to estimate the diffusion tensor and through this estimation obtain the ODF. The algorithm used to analyse the TriPGSEbp experiment data was used to draw ODFs of simulated data to test the angular resolution, resilience to noise, and ability to resolve a disc-shaped ODF constructed of 1000 prolate tensor structures. All simulations of data was performed in Matlab. The simulated data was based on a diffusion tensor of $D_{iso} = 10^{-9}$ m^2/s and $D_\Delta = 0.8$ or, for the test of angular resolution, $D_\Delta = 0.83$. Simulation of the signal and reconstruction of the ODF was performed using acquisition parameters of $b = 5 \cdot 10^9$[0.01 0.2 0.5 0.75 1] s/m^2/, b_Δ = [0 0.96] and $N_{dir} = 51$. This signal was then used to test different sets of b-parameters and number of directions in which to analyse the sample. As one acquisition of NMR data using the triple-stimulated spin-echo sequence for each value of b, b_Δ, and direction the total number of acquisitions, N, will be the product of the number of directions, N_dir, and the number of b- and b_Δ values. In order for the test to be feasible to useful in clinical applications a limitation of N was put to around 512. The testing resulted in the following parameters that were used to define the gradients using an in-house made Matlab script to adopt the b-matrix and defined directions into steering parameters for the gradient coils in the NMR spectrometer probe for the TriPGSTEbp-experiment. b_{rel} gives the relative values as compared to the maximum gradient strength of the spectrometer that must be adapted to each sample in order to obtain proper signal

attenuation.

$$b_{\text{rel}} = \begin{pmatrix} 0.01 \\ 0.2 \\ 0.5 \\ 0.75 \\ 1 \end{pmatrix}$$

$$b_{\Delta} = \begin{pmatrix} 0.98 \\ 0 \end{pmatrix}$$

$$N_{\text{dir}} = 51$$

6.2 AOT/H_2O/iso-octane sample preparation

As a model system, liquid crystals of 10 % w/w D_2O in H_2O (Milli-Q quality), iso-octane (Fluka AG) and detergent sodium 1,4-bis(2-ethylhexoxy)-1,4-dioxobutane-2-sulfonate (analytical grade, Sigma-Aldrich, Sweden) with the trade name Aerosol OT or AOT mixed in proportions to generate a reversed hexagonal phase at room temperatures. Proportions were based on the ternary phase diagram shown figure 6.1 and mixed in proportions shown in table 6.1 and as crosses in figure 6.1. All samples were mixed in 15 mL centrifuge tubes and centrifuged in alternating direction (cap-up/cap-down) for 2 minutes per direction in 25^{o}C in 2400 rpm until a homogenous mixture was achieved. About 500 μL of each sample was put into 5 mm NMR tubes which were centrifuged at 3300 rpm at 25^{o}C for 2 minutes.

Sample	H_2O/D_2O / (w/w %)	AOT / (w/w %)	iso-octane / (w/w %)
A	45	40	15
B	35	45	15

TABLE 6.1: Weight percent ratios of the studied liquid crystal samples.

Also, a sample of $C_{14}E_5$ mixed to 61.8 % w/w with D_2O in H_2O solution was lent by Professor Topgaard whom had prepared the sample to form concentric circular channels according to the protocol described in [19].

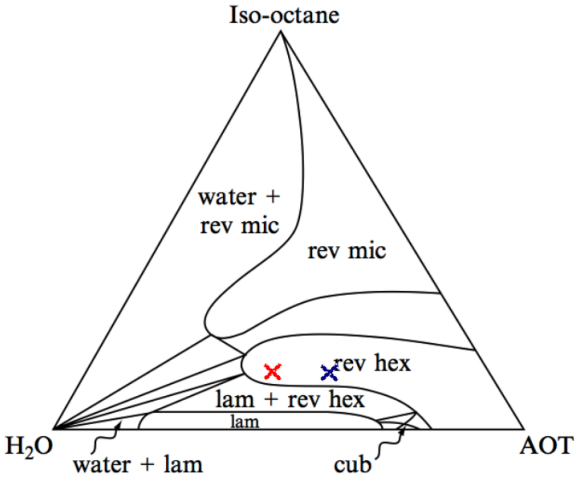

FIGURE 6.1: Ternary phase diagram marked with the selected mass percentage ratios for the made samples. The red cross marks the ratio of the A sample while B is marked by the blue cross. Figure adopted from [36]

6.3 NMR measurements

All NMR experiments were performed on a Bruker Avance-II 500 MHz spectrometer with an 11.7 T magnet equipped with a Bruker MIC-5 microimaging probe giving maximum magnetic field gradients of 3 T/m in three orthogonal directions (Bruker, Germany). Spectrometer data were processed using the standard spectrometer software TopSpin 2.1 (Bruker, Germany) and Matlab. The liquid crystalline phase structure was determined by recording ^{2}H NMR spectra using a probe fitted with a 5 mm ^{2}H/^{1}H RF insert. Relaxation rates were measured by standard T_1 inversion recovery and T_2 measuring spin echo experiments. All NMR measurements were performed at 18.4^{o}C.

6.3.1 Triple-stimulated spin-echo experiment

The maximum value of G was on the order of 0.5 T/m and adjusted for the different samples to reach reasonable signal attenuations. The b-matrix was defined in accordance with the obtained values under "Simulations" 6.1. Timing values used were $\delta = 0.6$ ms, $\Delta = 671.2$ ms, $\epsilon = 0.1$ ms, $\tau = 0.2$ ms, $\tau_1 = 1.2$ ms, and $\tau_2 = 670$ ms. τ_e used was 1 ms for sample A and C and 2 ms for sample B. The experiment was also repeated on a sample of free 10 % w/w D_2O in H_2O with the same settings of timing parameters

except a set τ_e of 2 ms. The b-space used was also the same except that only 5 directions were used.

The time-domain signals were converted to frequency spectra using Fourier transformation and subsequently phase corrected and baseline corrected using Matlab scripts coded in the department of Physical Chemistry at Lund University. The powder-averaged water signal $S(b, b_\Delta)$ was analysed using a least-square fitting Matlab routine "lsqcurvefit" to equation 3.21 with the adjustable parameters of initial signal intensity S_0, the isotropic diffusivity, D_{iso}, and the diffusion tensor anisotropy, D_Δ. Initial guesses for the fitting was both done from D_Δ=-0.47 and 0.98 and the best fit was chosen. The fitting was repeated for 10000 randomly chosen data sets acquired through use of bootstrap resampling [39].

Using in-house Matlab scripts, an ODF was produced by least-square fitting with a non-negativity constraint of the signal attenuation to a kernel based on the D_{eff} as described in equations 4.1 to 4.3.

6.3.2 Diffusion Tensor Imaging

To be able to compare the data from the triple-stimulated spin-echo pulse sequence with bipolar gradient pulse pairs, high resolution DTIs were obtained through the single-stimulated echo with bipolar pulse pairs experiment [19]. In order to compensate for signal loss due to substantial T_2 relaxation, an imaging sequence measuring T_2 values for each voxel was performed with the same imaging settings as for the standard DTI.

The DTI data was interpreted and visualised using in-house Matlab scripts that calculate and plot CL, CP, and Diffusion tensor element xx, yy, and zz, values in each voxel. This shows the colour-coded directions of normalised values of the linear anisotropy, the direction of the normal vector to the planar anisotropy, and the directions of the diffusion tensor elements, respectively. CL and CP are calculated as shown in equations 2.13 and 2.14, respectively. Thereafter, an ODF was constructed by from masked values from the DTI to extract only the data not severely affected by T_2 relaxation. The DTI data chosen to produce the ODF was the λ_1-associated eigenvector for the assumed prolate samples, A and B, and the λ_3-associated eigenvector for the assumed oblate sample, C.

7. Results

7.1 Simulations

Data from the TriPGSTEbp experiment can be used to estimate the diffusion tensor and through this estimation obtain the ODF. The algorithm used to analyse the TriPGSEbp experiment data was used to draw ODFs of simulated data to test the angular resolution, resilience to noise, and ability to resolve a disc-shaped ODF constructed of 1000 prolate tensor structures. Figure 7.1 shows estimated D_Δ values and true and reconstructed ODFs of two channels separated by an angle. At 36^o separation, the reconstructed ODF start to become unable to resolve the channels. The sensitivity to noise is shown in figure 7.2 which shows that the accuracy of D_Δ estimation and ODF reconstruction increases with increasing SNR. Reconstruction of a disc shaped ODF shows a certain exaggeration of some directions than others.

7.2 NMR Characterisation of Lyotropic Liquid Crystal Samples

The resulting spectra resulting from Fourier transform of 90^o-acquire experiment data using the 1H and 2H probe of the AOT/H_2O/iso-octane samples are shown in figures 7.4 to 7.5. The relative height of the water peak compared to the peaks at lower frequency from AOT and iso-octane are as would be expected between the A and B samples as A has a higher relative water content. The deuterium spectra clearly show that the samples are in the reverse hexagonal phase. The total peak-to-peak width in the deuterium spectra are smaller for the A sample than for the B sample. Proton and deuterium spectra for sample C are found in figures 7.6 and 7.7, respectively.

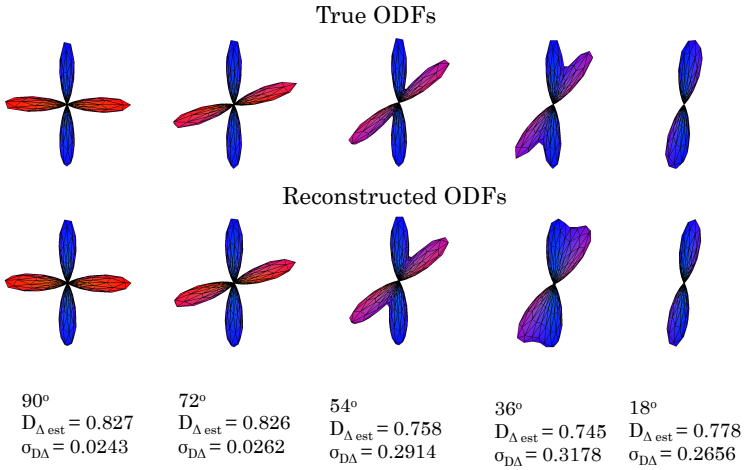

FIGURE 7.1: ODF reconstruction of two channels separated by 5 different angles, equally distributed from 90 to 18 degrees. True ODFs are shown in the top row while the reconstructed ODFs are shown below for each angle of separation. Colour in the ODF shows orientation, red and blue correspond to orientations parallel to the x-axis and z-axis, respectively. The separate orientations are distinguishable to some degree at 36 degrees but completely indistinguishable at 18 degree separation. Simulation of the signal and reconstruction of the ODF was performed using acquisition parameters of $b = 5 \cdot 10^9[0.01\ 0.2\ 0.5\ 0.75\ 1]$, $b_\Delta = [0\ 0.96]$ and $N_{dir} = 51$. $D_{\Delta est}$ and $\sigma_{D\Delta}$ show the estimated D_Δ and the standard deviation of the estimation, respectively. Also, noise was added to an extent which granted a signal to noise ratio of 50.

Table 7.1 shows the population weighted mean relaxation times for the studied samples. As the sample consists of domains with different orientations of anisotropic water diffusion structures, T_2 will depend greatly on the orientation along which the signal is measured. T_2 measurements were not performed on sample C. Sample A has slightly higher population weighted mean T_1 and T_2 values than sample B.

Sample	T_1 / (s)	T_2 / (ms)
A	1.38	15
B	1.11	11
C	1.80	NA

TABLE 7.1: T_1 and population weighted mean T_2 values of water in the studied samples.

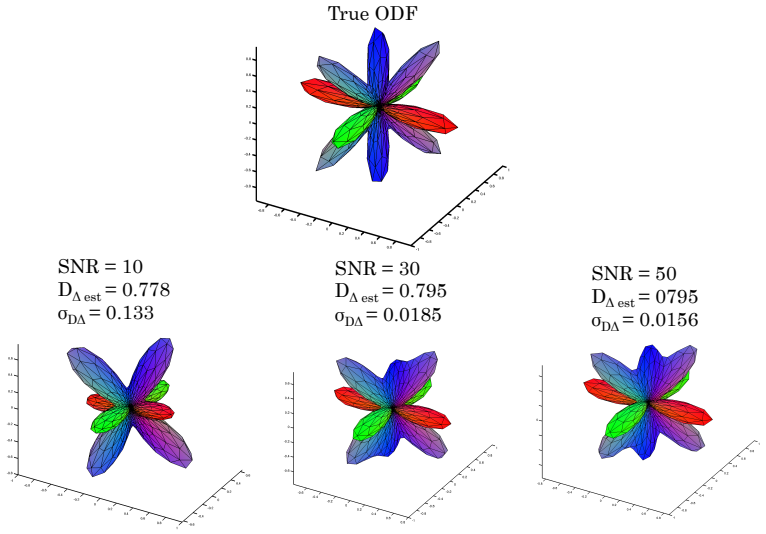

FIGURE 7.2: A simulated ODF with 5 channel orientations shown in the top reconstructed after added noise to provide simulated data of signal to noise ratios of 10, 30 and 50, as shown above the reconstructed ODFs. Colour in the ODF shows orientation, red, green and blue correspond to orientations parallel to the x-axis, y-axis and z-axis, respectively. $D_{\Delta\text{est}}$ and $\sigma_{D\Delta}$ show the estimated D_Δ and the standard deviation of the estimation, respectively. At low signal to noise ratio, the z direction is completely lost and the relative sizes of the channel directions are skewed and the standard deviation of the estimated D_Δ is large. Simulation of the signal and reconstruction of the ODF was performed using acquisition parameters of $b = 5 \cdot 10^9[0.01\ 0.2\ 0.5\ 0.75\ 1]$, $b_\Delta = [0.96\ 0]$ and $N_{dir} = 51$.

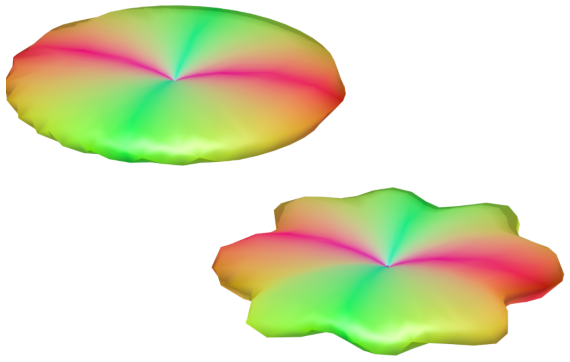

FIGURE 7.3: Reconstruction of the ODF of a disc of 1000 water channels in an evenly distributed in the x-y-plane was performed using acquisition parameters of $b = 5 \cdot 10^9[0.01\ 0.2\ 0.5\ 0.75\ 1]$, $b_\Delta = [0.96\ 0]$ and $N_{dir} = 51$. The true D_Δ, 0.8, was estimated to 0.79 with a standard deviation of 0.0388. Colour in the ODF shows orientation, red, green and blue correspond to orientations parallel to the x-axis, y-axis and z-axis, respectively. Also, noise was added to an extent which granted a signal to noise ratio of 50. The effects of a limited number of directions and a prolate diffusion tensor are seen as edges sticking out in the circle.

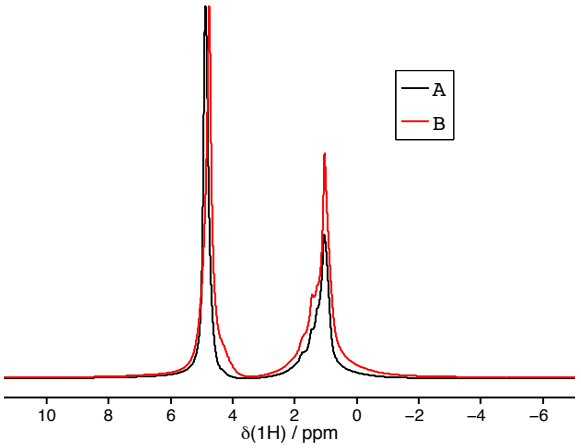

FIGURE 7.4: Proton spectra of the studied AOT/H_2O/iso-octane samples acquired using a 90-acquire NMR pulse sequence experiment. Black line shows the A-sample, of higher water content, and the red line shows the B-sample, of lower water content.

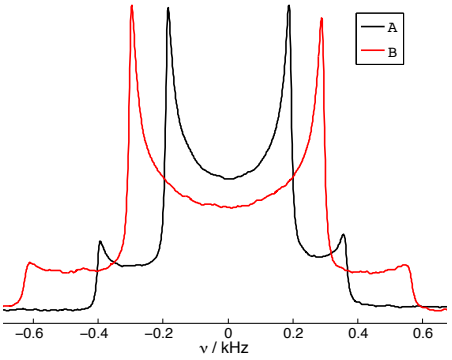

FIGURE 7.5: Deuterium spectra of the studied AOT/H_2O/iso-octane samples acquired using a 90-acquire NMR pulse sequence experiment. Black line shows the A-sample, of higher water content, and the red line shows the B-sample, of lower water content.

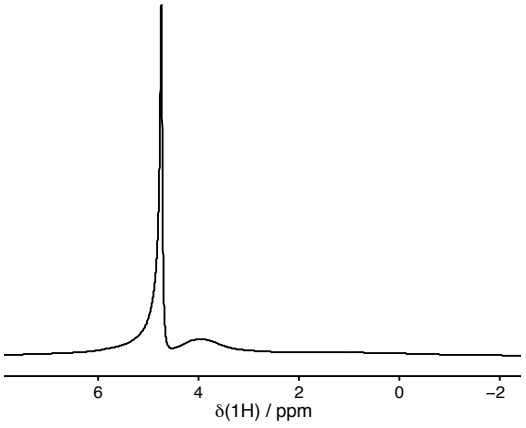

FIGURE 7.6: Proton spectrum of sample C acquired using a 90-acquire NMR pulse sequence experiment.

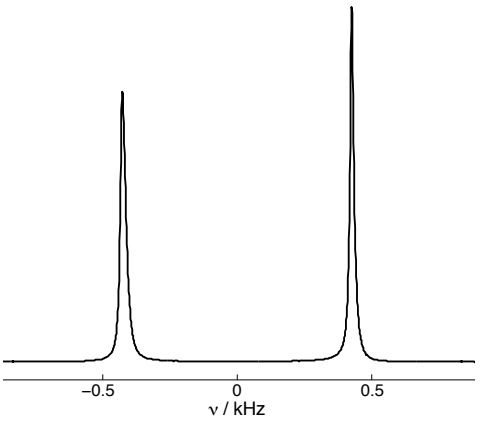

FIGURE 7.7: Deuterium spectrum of sample C acquired using a 90-acquire NMR pulse sequence experiment.

7.3 Diffusion tensor estimations & ODF reconstruction

Table 7.2 show the results of the fit of data from the TriPGSTEbp experiment to the equation 3.22. The data points and fitted curves are shown in figure 7.8. It should also be noted that the normalised signal intensity plotted as a function of b-values are clearly separated for the two b_Δ for higher b-values which indicates a high level of anisotropy. The theoretical connection between $D_\perp$, $D_\parallel$ and D_{iso} and D_Δ shown in 2.8 and 2.9 was used to calculate values to compare with the parameter estimation of the fit of the same data to equation 3.21. For samples A and B the axial diffusion coefficient was much greater than the radial whilst for sample C, the radial was greater than the axial. The 10 % w/w D_2O in H_2O sample, results of TriPGSTEbp experiment shown in figure 7.9, shows isotropic diffusion characteristics. The $D_\parallel$ and $D_\perp$ value of free water was higher than that for the lyotropic liquid crystal samples. Samples A and C show a higher mean diffusion than the B sample.

Sample	MD / (m^2/s)	AD / (m^2/s)	RD / (m^2/s)	D_{iso} / (m^2/s)	D_Δ
A	$3.70 \cdot 10^{-10}$	$1.10 \cdot 10^{-9}$	$3.30 \cdot 10^{-11}$	$3.73 \cdot 10^{-10}$	0.91
B	$2.90 \cdot 10^{-10}$	$8.10 \cdot 10^{-10}$	$2.70 \cdot 10^{-11}$	$2.88 \cdot 10^{-10}$	0.91
C	$7.6 \cdot 10^{-10}$	$4.5 \cdot 10^{-11}$	$1.10 \cdot 10^{-9}$	$7.65 \cdot 10^{-10}$	-0.47
10 % w/w D_2O in H_2O	$1.98 \cdot 10^{-9}$	$1.98 \cdot 10^{-9}$	$1.98 \cdot 10^{-9}$	$1.98 \cdot 10^{-9}$	0.00

TABLE 7.2: Mean, axial and radial diffusion coefficients from fitting of TriPGSTEbp experiment data on samples A-C and a sample of 10 % w/w D_2O in H_2O for comparison.

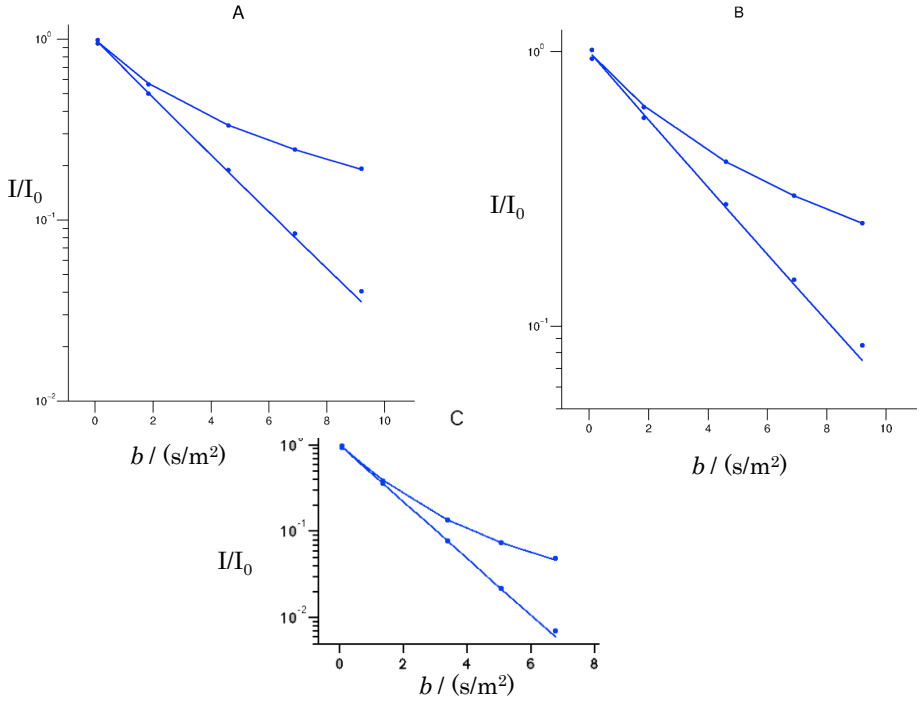

FIGURE 7.8: Normalised signal intensity, I/I_0 vs. the total diffusion weighting, b, with fitted curves to equation 3.21 for sample A, B, or C.

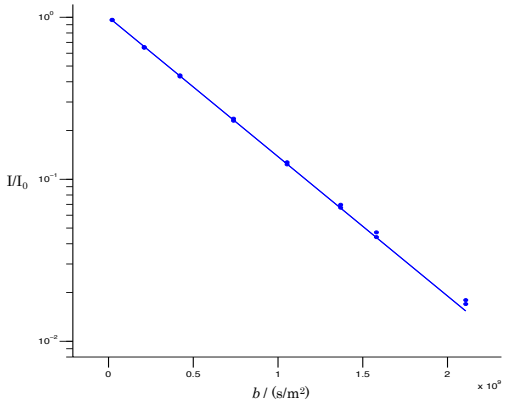

FIGURE 7.9: Normalised signal intensity, I/I_0, vs. the total diffusion weighting, b, with fitted curves for the 10 % w/w D_2O in H_2O sample.

Table 7.3 shows the fitted parameters, D_{iso} and D_Δ, to equation 3.21. The D_{iso} values of sample C are greater than the B and A samples. A and B samples show D_Δ values that show a clear prolate diffusion tensor while the sample C shows an oblate tensor.

Graphical representations of the diffusion tensors are included in figures 7.10 to 7.12 diffusion tensor images are shown to the left and the constructed ODF from the DTI experiment, masked by results from T_2-imaging, shown to the right of the DTIs, is shown

Sample	D_{iso} / (m^2/s)	D_Δ
A	$3.69 \pm 0.03 \cdot 10^{-10}$	0.90 ± 0.02
B	$2.77 \pm 0.02 \cdot 10^{-10}$	0.90 ± 0.01
C	$7.63 \pm 0.1 \cdot 10^{-10}$	-0.48 ± 0.05

TABLE 7.3: D_{iso} and D_Δ values from fitting of triple stimulated echo experiment on samples A-C. The uncertainties correspond to 95% confidence interval as determined with bootstrapping.

on the top right. The constructed ODF from the triple stimulated echo-experiments is found in to the lower right in the figures. The shape of the diffusion tensors based on the estimations of the D_{iso} and D_Δ are included as elongated, prolate, or The diffusion tensor image show maps of, in order from left to right, the linear diffusion tensor, CL, the normal vector to the planar diffusion tensor, CP, and the diffusion coefficient in the tensor's PAS. The level of CL and CP in the figures give an estimate of how correctly the diffusion tensor can be assumed to have one shape. Sample A seems to have a majority of voxels having a high CL value, while sample B has a slightly more share of voxels showing a higher CL value. Sample C has one central channel clearly shown in the CL image and, due to the circularity of the lamellas, a high CP value in the rest of the sample. The ODFs from the different datasets are very similar. The ODFs from the TriPGSTEbp-data are slightly more spiny.

7.4 Test of Diffusion Coefficient Estimation

The diffusion coefficients of the 10 % w/w D_2O in H_2O sample shown in the lowest row of table **??** obtained through analysis of a TriPGSEbp experiment correspond to values extrapolated from values found in previously published data to 99.85% [40] [41]. This assumes that there is a linear correlation to the influence of D_2O on the self-diffusion coefficient of H_2O in a D_2O in H_2O mixture. No correction of the measured diffusion coefficients were deemed necessary.

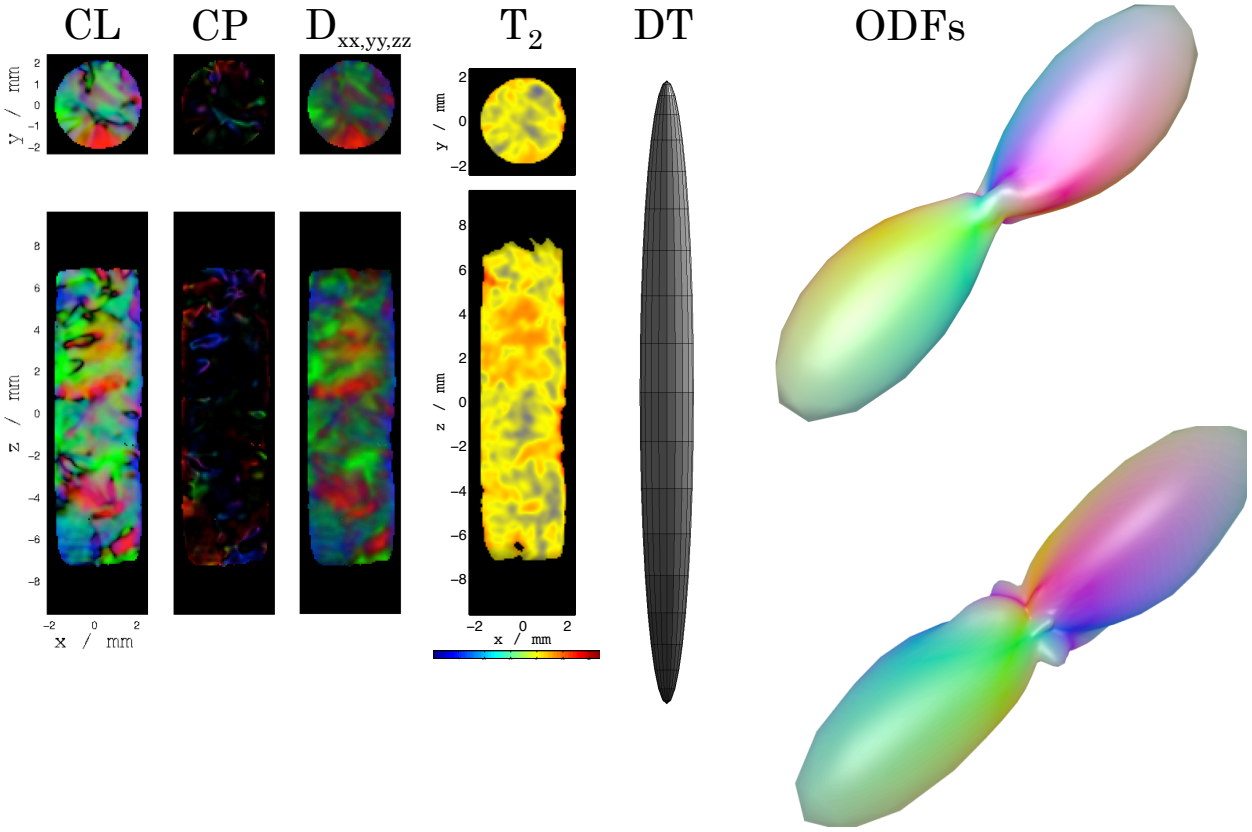

FIGURE 7.10: DTIs (left), T_2-image, shape of diffusion tensor (centre) and reconstructed ODFs (top based on T_2-weighted DTI data, bottom based on TriPGSEbp data) of sample A. Colours in the T_2-image is correlated to the value of T_2 in each voxel as a logarithmic scale between maximum 100 ms, blue, and 2 ms, red as indicated by the colourbar. The diffusion tensor shape is based on the D_Δ value. All colours in the figures are depending on the direction of either the diffusion tensor, DTIs, or the orientations, ODF. Red, green, and blue means x-, y-, and z-direction, respectively. The DTIs show the CL, CP, and directional diffusion tensor values, from left to right.

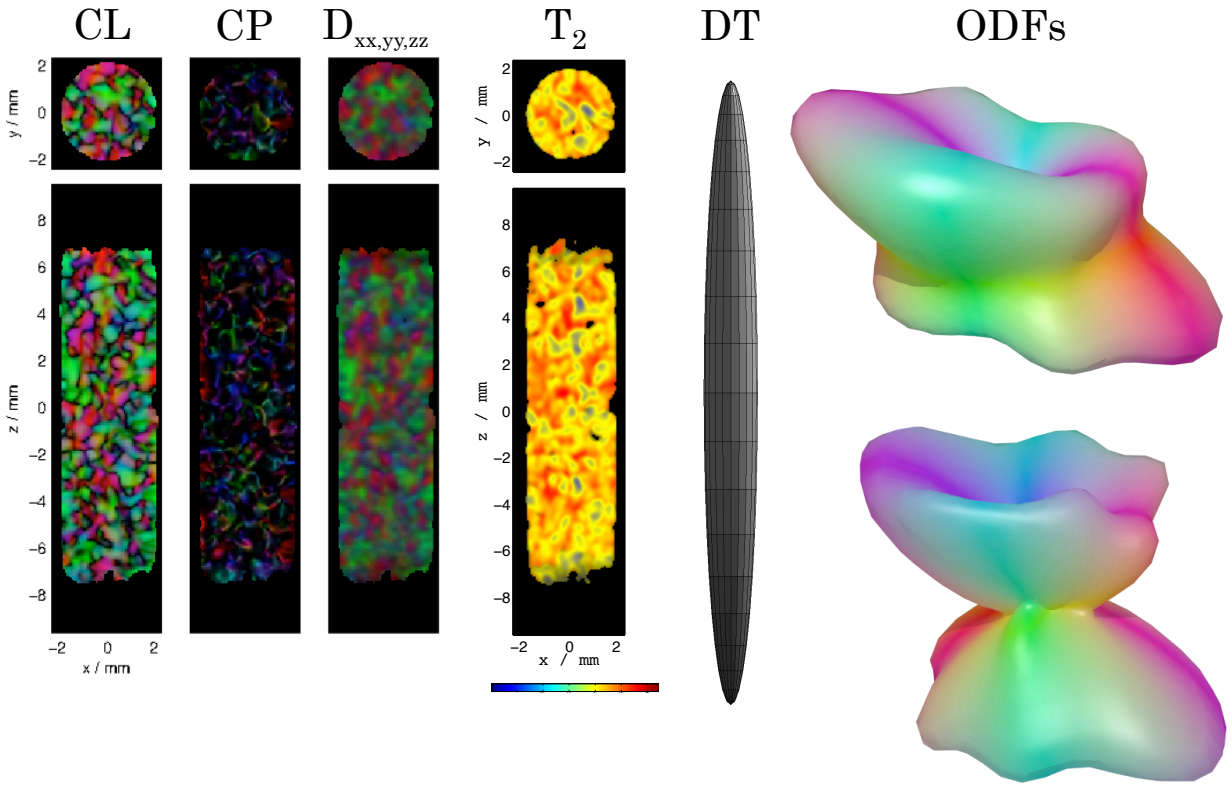

FIGURE 7.11: DTIs (left), T_2-image, shape of diffusion tensor (centre) and reconstructed ODFs (top based on T_2-weighted DTI data, bottom based on TriPGSEbp data) of sample B. Colours in the T_2-image is correlated to the value of T_2 in each voxel as a logarithmic scale between maximum 50 ms, blue, and 3.3 ms, red as indicated by the colourbar. The diffusion tensor shape is based on the D_Δ value. All colours in the figures are depending on the direction of either the diffusion tensor, DTIs, or the orientations, ODF. Red, green, and blue means x-, y-, and z-direction, respectively. The DTIs show the CL, normal vector of CP, and directional diffusion tensor values, from left to right.

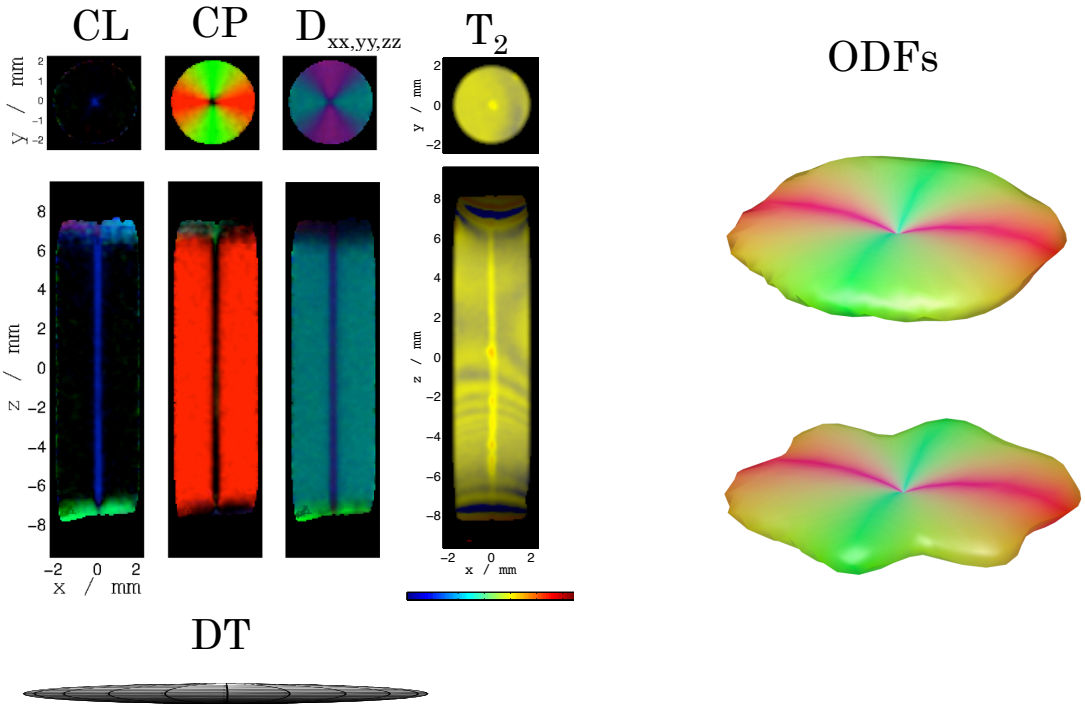

FIGURE 7.12: DTIs (left), T_2-image, shape of diffusion tensor (lower left corner) and reconstructed ODFs (top based on T_2-weighted DTI data, bottom based on TriPGSEbp data) of sample C. Colours in the T_2-image is correlated to the value of T_2 in each voxel as a logarithmic scale between maximum 1000 ms, blue, and 1 ms, red as indicated by the colourbar. The diffusion tensor shape is based on the D_Δ value. All colours in the figures are depending on the direction of either the diffusion tensor, DTIs, or the orientations, ODF. Red, green, and blue means x-, y-, and z-direction, respectively. The DTIs show the CL, normal vector of CP, and directional diffusion tensor values, from left to right.

8. Discussion

8.1 Simulations

The angular resolution of this technique is limited by the number of directions of the gradient frame, as the encoding of diffusion information is performed in these directions. Second, the angular resolution in the ODF reconstruction method used to produce the ODFs is limited by the choice of the number of points that build up the spherical mesh onto which the amplitude of the reconstructed ODF is projected. This is hardly the limiting factor for the simulations shown in the figure, however, since 1000 points evenly spaced rather densely covers the sphere.

The effects of different noise levels is shown in figure 7.2. A sample with many different directions of channels was chosen in order to put larger strain on the reliability of the reconstructed ODF. It is evident that the estimations of D_Δ increase in reliability with increasing SNR as the standard deviation of the estimations decrease with increasing SNR. The reconstructed ODFs show increasing similarities to the true ODF although, interestingly, the channel direction along the z-axis seems to be harder to resolve. This should be evaluated further to assess whether this is a systematic error that can be compensated for.

Simulation of 1000 evenly distributed channels in the x-y-plane is shown in figure 7.3. The over-estimated edges along some orientations in the plane is most probably due to the limited number of directions of the gradient frame that are measured as discussed regarding the angular resolution.

The use of simulations to get a first-glance estimate of the parameters of the diffusion-weighted matrix and test the limits of data analysis is indeed very useful. However, for

diffusion weighted experiments it is limited by how well-described the theoretical signal attenuation profile is.

8.2 Lyotropic Liquid Crystals

The AOT/H_2O/iso-octane lyotropic liquid crystals are suitable as model systems as they are cheap to produce, relatively well studied and easy to mix into reverse hexagonal phase. For future experiments, amphiphilic molecules specialised for desired function could be used. For instance, amphiphilic molecules with higher anisotropic magnetic susceptibility would cause a higher degree of orientation along the tube length, which could serve as an interesting test sample for future dMRI-experiments. Alternatively, the sample could be allowed to be affected by the strong magnetic field for a longer period of time. Also, possibly, diffusion NMR could be used to study functionally designed lyotropic crystalline structures to measure transport through lamellar barriers or between rods in reverse hexagonal phase. This could be a useful alternative as a first step to study diffusion effects in biological samples as the lyotropic crystals might be more stable over time than cells.

Figure 7.6 shows the proton spectrum of samples A and B. The water peak is visible at 4.7 ppm chemical shift for both samples. The relative height of the water peak as compared to other peaks in the spectrum is larger in the spectrum for sample A than to sample B. This is to be expected as the relative water content of sample A is higher than that for sample B, as can be seen in table 6.1.

Deuterium spectra can be used to observe the phase of the lyotropic liquid crystal structures [1, 28]. The deuterium spectra of the A and B-samples, shown in figure 7.5, show clear anisotropic phase, which was exactly as wanted and is in accordance to the literature for the studied concentration ratios between AOT, H_2O and iso-octane [36] . If the main axis of symmetry of the liquid crystal, i.e. the channels or lamellas, is along the same axis as for the B_0-field, the width of the quadropolar splitting is more narrow than if the axes are in some angle. This could be explained, observing the ODFs and DTIs in figures 7.10 and 7.11, as a consequence of a higher variety of directions in sample B. The shoulder peaks of sample A are more pronounced than those for sample B in the deuterium spectra. This might be due to fewer orientations of channels in sample

A than in sample B which would give less spread in the quadropolar splitting. Figures 7.6 and 7.7 shows the proton and deuterium spectra of sample C, respectively. The deuterium spectrum shows that the lyotropic liquid crystal structures are anisotropic and of extremely highly uniform direction, as is confirmed by the DTI images in figure 7.12.

The T_2 relaxation constants of water shown in table 7.1 are measured in one direction but due to the anisotropy within the sample, the values will be a population-weighted average. These values should be compared to the T_2-images found in figures 7.10 to 7.12 which show that the spread of T_2-values are great in samples A and B but less in sample C.

8.3 Diffusion Tensor Estimations

The mean, axial, and radial diffusion coefficients, shown in table 7.2 of the studied samples show that the samples show anisotropic diffusion coefficients. Specifically, samples A and B show highly prolate diffusion tensors while sample C shows an oblate diffusion tensor. It is worth noticing that the signal attenuation of the B sample is poorer than for the A sample and the C sample. This might be an effect of too strong or too weak diffusion encoding gradients being used. Too low gradient field strength would not cause enough signal attenuation while too high would risk that the attenuation would be too high, risking the signal becoming too noisy to analyse. While measuring, it could be observed that the signal was very low for the highest b-values, making the case of too high b-values implausible. It is worth noticing that the lowest relative b-value is not zero but 1%. When using strong enough gradients, this might cause differences in signal attenuations for the lowest b-values at the different diffusion encoding angles. This would explain the small differences that can be seen in relative signal for samples A, B, and C, most pronounced on measurements on sample B. For future studies, it should be studied if the minimum relative b-values could be decreased further, without risking too many artefacts [15]. The effect of too low signal attenuation would be that the D_{iso} value might be underestimated and that the D_{Δ} value would be harder to determine since the difference in signal attenuation is lower for stronger gradients. In future experiments, the signal attenuations should be more thoroughly controlled after each

measurement. The measurements on the sample of free water shows perfect isotropic diffusion characteristics.

The $D_{\text{iso}}/D_{\Delta}$ parameterisation fit function seems to work well as the fitted values seem to be within acceptable spread. Comparing the calculated D_{iso} and D_{Δ} values from the fitted MD, AD, RD-values to the fitted values show that the fit function strategy used in the analysis algorithm for obtaining the D_{iso} and D_{Δ}-values is suitable. By guessing for both prolate and oblate diffusion tensors at each round of fitting in the Bootstrap loop, both prolate and oblate tensors can be detected. This is explicitly shown by the analysis of sample C which, due to the oriented lamellar layers showcase a near perfect oblate diffusion tensor.

8.4 Orientation Distribution Function Reconstruction

The reconstructed ODFs from the TriPGSEbp experiment, shown together with calculated diffusion tensor shape and DTI images in figures 7.10 to 7.12 , generally accentuate the directionality of the channels more than those reconstructed from T_2-masked DTI data. Looking at the reconstruction of the ODF of simulated data of a disc shape shows that, probably due to the limited number of measurement directions, this accentuation seems to be inherent in the mesh-based ODF reconstruction method. The method still seems to be appropriate due to the, relatively, simple approach and the decreased need of hands-on reconstruction manipulations to fulfil the criteria of the ODF being real and non-negative compared to other spherical deconvolution methods.

The ODF reconstruction is based on the eigenvector associated with the largest or smallest eigenvalues of the T_2-masked DTI data or the D_{eff} for the TriPGSEbp data. In the reconstruction of the ODF from the DTI experiment the direction of the vector along which axial symmetry is formed is used in order to reconstruct the ODF in a randomly selected representative subset of the DTI data. This is true for the prolate tensors while for the oblate tensors, the direction of the channels will be the least dominant eigenvector, associated to the direction of the diffusion perpendicular to the channel. The decision of which vector to base the ODF on from the DTI experiment must be decided before producing the ODF, which is not needed for the TriPGSTEbp-data. It can be seen in the DTI of sample B that planar voxel-averaged tensor domains are also

present. Even if this should not affect the ODF reconstruction because of the choice of prolate tensor data, it might cause a lower SNR. Also, too strong gradients would generate noisy signals which might cause detections of false directions in the ODF. Hence, sufficient SNR should be ensured in the measurements.

If this technique is to be used to track the orientation of nerve fibers, the matter of angular accuracy must be analysed [11, 42]. Even if the angular deviation between the reconstructed ODF and the true fiber direction is small, if the error is systematic then it follows that the accumulated deviation will lead the fiber tracking algorithm astray. Samples with well known orientations of millimetre-length structures should be analysed and the algorithm corrected to account for known deviations.

8.5 Triple-stimulated echo-sequence

It is evident that the triple-stimulated echo experiment shows great promise to be used to study samples with short T_2-times such as the lyotropic liquid crystal systems studied in this work.

Diffusion MRI techniques encoding diffusion both directionally and isotropically can be used to distinguish between tumours in different tissues [4]. The TriPGSTEbp experiment can provide reliable estimations of the shape of the diffusion tensor, especially distinguishing between oblate and prolate shapes, and from the data an accurate fibre ODF based on the shape of the diffusion tensor can be calculated. A logical next step would be to evaluate a pulse sequence based on being able to vary b_Δ on neuronal tissue using a clinical MRI scanner to evaluate the ODF reconstruction strategy using D_{eff} for DTI and fiber tracking applications, possibly providing more clinically meaningful information regarding the anatomy of analysed tissues. For this, a suitable balance between the number of diffusion encoding directions and number of values of b and b_Δ should be produced. The best balance of these parameters would be dependent on which information is desirable to assess. Varying b_Δ to more values would provide a better estimation of the shape of the diffusion tensor while an increased number of encoding directions could improve the angular resolution of the ODF.

The technique is useful for studying lyotropic liquid crystals and it is shown that the data obtained can, using relatively few sequence acquisitions, be effectively used to estimate

the diffusion tensor elements and ODF of the sample. An alternative to simulations to obtain a guess of a vector of relative b- and b_Δ-values to use would be to measure an excess of b-matrix settings and in the analysis try out which subset of parameters give the most efficient fitting. This strategy would be very time-consuming but useful in complex samples where the reliability of the simulated data might be questionable due to simplifications in the diffusion tensor and ODF specifications. This is especially true if concern should be given to samples containing domains of more than one kind of diffusion characteristics. As lyotropic liquid crystal systems are investigated as possible materials for controlled release systems, diffusion profiles are of growing importance [43]. The TriPGSTEbp-experiment could provide a more detailed estimation of the diffusion profile within the carrier structures that might be of use for testing new approaches of drug delivery systems [44, 45]. This will be of growing importance as drug delivery systems grow more complex. Also, TriPGSTEbp could be used to study other molecular diffusion than water. Larger molecules would require longer times for diffusion which would mean a higher sensitivity T_2-relaxation which might cause problems for diffusion encoding in multiple directions. However, there might be time-resolution benefits in the measurements if this could be circumvented. The ODF could be of interest if complex drug delivery systems include structures in which water is supposed to be able to enter and transport through some drug delivery material in an ordered fashion.

9. Conclusions

The work in the thesis project accounted for in this report examines a diffusion weighted experiment, the triple-stimulated pulse echo experiment, which encodes diffusion both directionally and isotropically. The possibility of the latter is a recent discovery and makes it possible to obtain direct information of the shape of the diffusion tensor, which describes how water can diffuse inside of the studied sample. This is shown by studying three samples of lyotropic liquid crystal systems, prepared in ways as to show lamellar or channel structures on the nano- to millimetre scale. The experiment was repeated in multiple directions of diffusion encoding. This allows for a more correct diffusion tensor estimation as the signals are measured along more of the water channel directions, hence, when averaged for all directions, providing a more representative measurement. Moreover, the multiple directions measured also provides the necessary data to produce a three dimensional map of the microscopic crystalline structure, the orientation distribution function (ODF). The number of encoding directions and variations of the parameters tuning the diffusion encoding gradients are restricted to show that the techniques are feasible to use in practical applications, as each extra parameter setting equals one extra measurement adding to the total time needed for the experiment. The major finding of this thesis work is that the diffusion tensor shape and the ODF can be determined from the data of a single diffusion-weighted NMR experiment and that the diffusion tensor can be used in the estimation of the ODF directly. Of special importance is that the technique can be used to determine whether the diffusion tensor is oblate, i.e. lentil shaped, or prolate, i.e. cigarr-shaped. This is shown explicitly by measurements on samples containing regions of water channel structures and concentric lamellar water planes with subsequent data analysis.

For future work, an optimised balance between the number of diffusion encoding directions and parameters governing the diffusion encoding magnetic gradients, which

together make up the total number of scans needed and thus the time the experiment consumes, should be produced. This means somewhat of a tradeoff between optimising for estimating the diffusion tensor, which improves with more tested parameters of diffusion encoding magnetic gradients, and calculation of ODF, which would gain in resolution from more number of diffusion encoding directions. Moreover, samples that show more complex diffusion patterns can be studied in order to check the possibility of detecting these diffusion profiles and still gaining a correct ODF, which should be theoretically possible using the same strategy as described in this report as long as the signal attenuation due to diffusion can be theoretically described. The experiment could also be introduced into a clinical setting to gain more insight in the structure of the microstructure of tissues without the need of guessing the diffusion characteristics beforehand.

Bibliography

[1] T. M. Ferreira, D. Bernin, and D. Topgaard. Nmr studies of nonionic surfactants. *Ann. R. NMR. S.*, 79:73–127, 2013.

[2] K. Santhosh, B. Thomas, V. V. Radhakrishnan, J. Saini, C. Kesavadas, A. K. Gupta, T. R. Kapilamoorthy, and S. N. Nair. Diffusion tensor and tensor metrics imaging inintracranial epidermoid cysts. *'J. Magn. Reson. Im.*, 29:967–970, 2009.

[3] S. Lasic, F. Szczepankiewicz, S. Eriksson, M. Nilsson, and D. Topgaard. Microanisotropy imaging: quantification of microscopic diffusion anisotropy and orientational order parameter by diffusion mri with magic-angle spinning of the q-vector. *Front. Phys.*, 9:e98752, 2014.

[4] F. Szczepankiewicz, S. Lasic, D. van Westen, P. C. Sundgren, E. Englund, C.-F. Westin, F-Ståhlberg, J. Lätt, D. Topgaard, and M. Nilsson. Quantification of microscopic diffusion anisotropy disentangles effects of orientation dispersion from microstructure applications in healthy volunteers and in brain tumors. *NeuroImage.*, 104:241–252, 2015.

[5] Q. Min, K. Shao, L. Zhai, W. Liu, C. Zhu, L. Yuan, and J. Yang. Differential diagnosis of benign and malignant breast masses using diffusion-weighted magnetic resonance imaging. *World. J. Surg. Oncol.*, 13:32, 2015.

[6] J.-D. Tournier, S. Mori, and A. Leemans. Diffusion tensor imaging and beyond. *Magn. Reson. Med.*, 65:1532–1556, 2011.

[7] H. Zhang, P. L. Hubbard, G. J. M. Parker, and D. C. Alexander. Axon diameter mapping in the presence of orientation dispersion with diffusion mri. *NeuroImage*, 56:1301–1315, 2011.

[8] S.N. Jespersen, C.D. Kroenke, L. Ostergaard, J.J.H. Ackerman, and D.A. Yablonskiy. Modeling dendrite density from magnetic resonance diffusion measurements. *NeuroImage*, 34:1473–1486, 2007.

[9] S.K. Song, S. W. Sun, M.J. Ramsbottom, C. Chang, J. Russell, and A.H. Cross. Dysmyelination revealed through mri as increased radial (but unchanged axial) diffusion of water. *NeuroImage*, 17:1429–1436, 2002.

[10] J. D. Tournier, F. Calamante, D. G. Gadian, and A. Connelly. Direct estimation of the fiber orientation density function from diffusion-weighted mri data using spherical deconvolution. *NeuroImage*, 23:1176–1185, 2004.

[11] W. Zhan and Y. Yang. How accurately can the diffusion profiles indicate multiple fiber orientations? a study on general fiber crossings in diffusion mri. *J. Magn. Reson.*, 183:193–202, 2006.

[12] B. Jeurissen, A. Leemans, J.-D. Tournier, D. K. Jones, and J. Sijbers. Investigating the prevalence of complex fiberconfigurations in white matter tissue with diffusion magnetic resonance imaging. *Hum. Brain. Mapp.*, 34:2747–2766, 2013.

[13] J. Keeler. *Understanding NMR Spectroscopy.* John Wiley & Sons, Ltd, 2nd edition, 2010.

[14] D. Topgaard. Isotropic diffusion weighting using a triple-stimulated echo pulse sequence with bipolar gradient pulse pairs. *Micropor. Mesopor. Mat.*, 205:48–51, 2015.

[15] S. Eriksson, S. Lasic, M. Nilsson, C.-F. Westin, and D. Topgaard. Nmr diffusion-encoding with axial symmetry and variable anisotropy: Distinguishing between prolate and oblate microscopic diffusion tensors with unknown orientation distribution. *J. Chem. Phys.*, 142:104201, 2015.

[16] B. Jeurissen, J.-D. Tournier, T. Dhollander, A. Connelly, and J. Sijbers. Multi-tissue constrained spherical deconvolution for improved analysis of multi-shell diffusion mri data. *NeuroImage*, 103:411–426, 2014.

[17] L. Astola, A. Jalba, and E. Balmashnova. Fiber streamline tracking with single tensor orientation distribution function for high angular resolution diffusion imaging. *J. Math. Imaging. Vis.*, 41:170–181, 2011.

[18] I. Aslund, C. Cabaleiro-Lago, O. Soderman, and D. Topgaard. Diffusion nmr for determining the homogeneous length-scale in lamellar phases. *J. Phys. Chem. B*, 112:2782–2794, 2008.

[19] D. Bernin, V. Koch, and D. Topgaard M. Nyden. Multi-scale characterization of lyotropic liquid crystals using 2h and diffusion mri with spatial resolution in three dimensions. *PLOS ONE*, 9:e98752, 2014.

[20] S. Eriksson, S. Lasic, and D. Topgaard. Isotropic diffusion weighting in pgse nmr by magic-angle spinning of the q-vector. *J. Magn. Reson.*, 226:13–18, 2013.

[21] P. J. Basser, J. Mattiello, and D. LeBihan. Mr diffusion tensor spectroscopy and imaging. *'Biophys. Chem.*, 66:259–267, 1994.

[22] C. Pierpaoli and P. J. Basser. Toward a quantitative assessment of diffusion anisotropy. *Magn. Reson. Med.*, 36:893–906, 1996.

[23] D. Topgaard and O. Söderman. Self-diffusion in two- and three-dimensional powders of anisotropic domains: an nmr study of the diffusion of water in cellulose and starch. *J. Phys. Chem. B*, 106:11887–11892, 2002.

[24] P. J. Basser and C. Pierpaoli. Microstructural and physiological features of tissues elucidated by quantitative-diffusion-tensor mri. *J. Magn. Reson.*, 111:209–219, 1996.

[25] D. W. McRobbie, E. A. Moore, M. J. Graves, and M. R. Prince. *MRI From Picture to Proton*. Cambridge University Press, 2nd edition, 2006.

[26] W. S. Price. Applications of pulsed gradient spin-echo nmr diffusion measurements to solution dynamics and organization. *Diffusion Fundamentals*, 2(112):1–19, 2005.

[27] W. S. Price. *Pulsed-Field Gradient Nuclear Magnetic Resonance as a Tool for Studying Translational Diffusion*, volume 9. 1997.

[28] D. Bernin, V. Koch, M. Nyden, and D. Topgaard. Multi-scale characterization of lyotropic liquid crystals using 2h and diffusion mri with spatial resolution in three dimensions. *PLOS ONE*, 9:e98752, 2014.

[29] X. Li, L. X, W. Chen, F. Liu, S. Crozier, and D. Xie. Finite element analysis of gradient z-coil induced eddy currents in a permanent mri magnet. *J. Magn. Reson.*, 208:148–155, 2011.

[30] M. Bak and N. C. Nielsen. Repulsion, a novel approach to efficient powder averaging in solid-state nmr. *J. Magn. Reson.*, 125:132–139, 1997.

[31] C. Guissani, A. Poliakov, R. T. Ferri, L. L. Plawner, S. R. Browd, D. W. W. Shaw, T. Z. Filardi, C. Hoeppner, J. R. Geyer, J. M. Olson, J. G. Douglas, E. H. Villavicencio, R. G. Ellenbogen, and J. G. Ojemann. Dti fiber tracking to differentiate demyelinating diseases from diffuse brain stem glioma. *NeuroImage*, 52:217–223, 2010.

[32] D. S. Tuch, T. G. Reese, M. R. Wiegell, and V. J. Wedeen. Diffusion mri of complex neural architecture. *Neuron*, 40:885–895, 2003.

[33] L. R. Frank. Anisotropy in high angular resolutiondiffusion-weighted mri. *Magn. Reson. Med.*, 40:885–895, 2003.

[34] M. Descoteaux, R. Deriche, T. R. Knösche, and A. Anwander. Deterministic and probabilistic tractography based on complex fibre orientation distributions. *IEEE. T. Med. Imaging.*, 28:269–286, 2009.

[35] V. Patel, Y. Shi, P. M. Thompson, and A. W. Toga. Mesh-based spherical deconvolution: A flexible approach to reconstruction of non-negative fiber orientation distributions. *NeuroImage*, 51:1071–1081, 2010.

[36] K. Holmberg, B. Jönsson, B. Kronberg, and B. Lindman. *Surfactants and polymers in aqueous solution.* John Wiley & Sons Ltd, 1998.

[37] M. E. Tousley, X. Feng, M. Elimelech, and C. O. Osuji. Aligned nanostructured polymers by magnetic-field-directed self-assembly of a polymerizable lyotropic mesophase. *Appl. Mater. Interfaces*, 6:19710–19717, 2014.

[38] M. E. Tousley, X. Feng, M. Elimelech, and C. O. Osuji. Phase behaviour of lyotropic liquid crystals in external fields and confinement. *Eur. Phys. J. Special Topics*, 222: 3053–3069, 2013.

[39] B. Efron and R. Tibshirani. Bootstrap methods for standard-errors, confidence intervals, and other measures of statistical accuracy. *Stat. Sci.*, 1:54–77, 1986.

[40] M. Holz, S. R. Heil, and A. Sacco. Temperature-dependent self-diffusion coefficients of water and six selected molecular liquids for calibration in accurate 1h nmr pfg measurements. *'Phys. Chem. Chem. Phys.*, 2:4740–4742, 2000.

[41] R. Mills. Self-diffusion in normal and heavy water in the range 1-45. *'J. Phys. Chem.*, 77:685–688, 1973.

[42] M.-A. Cote, G. Girard, A. Bore, E. Garyfallidis, J.-C. Houde, and M. Descoteaux. Tractometer: Towards validation of tractography pipelines. *Med. Imag. Anal.*, 17: 844–857, 2013.

[43] M. Cohen-Avrahami, A. I. Shames, M. F. Ottaviani, A. Aserin, and N. Garti. On the correlation between the structure of lyotropic carriers and the delivery profiles of two common nsaids. *Colloid. Surface. B*, 122:231–240, 2014.

[44] E. V. Mathias, J. Aponte, J. A. Kornfield, and Y. Ba. Properties of small molecular drug loading and diffusion in a fluorinated peg hydrogel studied by 1h molecular diffusion nmr and 19f spin diffusion nmr. *Colloid. Polym. Sci.*, 288:1655–1663, 2010.

[45] M.-A. Gagnon and M. Lafleur. Comparison between nuclear magnetic resonance profiling and the source/sink approach for characterizing drug diffusion in hydrogel matrices. *Pharm. Dev. Technol.*, 16:651–656, 2011.